

Recent developments in transport phenomena in Weyl semimetals

Pavan Hosur

Department of Physics, Stanford University, Stanford, CA 94305, USA

Xiaoliang Qi

Department of Physics, Stanford University, Stanford, CA 94305, USA

Abstract

The last decade has witnessed great advancements in the science and engineering of systems with unconventional band structures, seeded by studies of graphene and topological insulators. While the band structure of graphene simulates massless relativistic electrons in two dimensions, topological insulators have bands that wind non-trivially over momentum space in a certain abstract sense. Over the last couple of years, enthusiasm has been burgeoning in another unconventional and topological (although, not quite in the same sense as topological insulators) phase – the Weyl Semimetal. In this phase, electrons mimic Weyl fermions that are well-known in high-energy physics, and inherit many of their properties, including an apparent violation of charge conservation known as the Chiral Anomaly. In this review, we recap some of the unusual transport properties of Weyl semimetals discussed in the literature so far, focusing on signatures whose roots lie in the anomaly. We also mention several proposed realizations of this phase in condensed matter systems, since they were what arguably precipitated activity on Weyl semimetals in the first place.

1. Introduction to Weyl semimetals

The earliest classification of the forms of matter in nature, typically presented to us in our early school days, consists of *solids*, *liquids* and *gases*. High school physics textbooks and experience later teach us that solids can be further classified based on their electronic properties as *conductors* and *insulators*. They tell us that as long as the electrons in a solid are non-interacting, solids with partially filled bands are metals or conductors while those with no partially filled bands and a gap between the valence and the conduction bands are insulators or semiconductors. Solid state physics courses in college add another phase to this list: if the gap is extremely small or vanishing, or if there is a tiny overlap between the valence and the conduction bands, the material is *semimetallic* and has markedly different electronic properties from metals and insulators. Graphene (Geim and Novoselov [11]) – a two dimensional (2D) sheet of carbon atoms – is the most celebrated example of a semimetal with a vanishing gap. In this system, the conduction and valence bands intersect at certain points in momentum space known as Dirac points. The dispersion near these points is linear and electrons at nearby momenta act like massless relativistic particles, thus stimulating the interest of condensed matter and high-energy physicists alike.

In the last couple of years, there has been growing interest in a seemingly close cousin of graphene – the so-called *Weyl semimetal* (WSM) (Wan et al. [38], Witczak-Krempa and Kim [42], Chen and Hermele [6], Turner and Vishwanath [33], Vafeek and Vishwanath [35], Volovik [37], Heikkila et al. [15]). Like graphene, its band structure has a pair of bands crossing at certain points in momentum space; unlike graphene, this is a three-dimensional (3D) system. Near each such *Weyl point* or *Weyl node*, the Hamiltonian resembles the Hamiltonian for the Weyl fermions

that are well-known in particle physics literature:

$$H_{\text{Weyl}} = \sum_{i,j \in \{x,y,z\}} \hbar v_{ij} k_i \sigma_j \quad (1.1)$$

where \hbar is the reduced Planck's constant, v_{ij} have dimensions of velocity, k_i is the momentum relative to the Weyl point and σ_i are Pauli matrices in the basis of the bands involved. Thus, the name *Weyl semimetal*.

A closer look, however, unveils a plethora of differences between graphene and WSMs because of their different dimensionality. An immediate consequence of the form of H_{Weyl} is that the Weyl points are topological objects in momentum space. Since all three Pauli matrices have been used up in H_{Weyl} , there is no matrix that anticommutes with H_{Weyl} and gaps out the spectrum. There are then only two ways a Weyl point can be destroyed. The first is by annihilating it with another Weyl point of opposite chirality, either by explicitly moving the Weyl points in momentum space and merging them or by allowing for scattering to occur between different Weyl nodes; the latter requires the violation of translational invariance. The second way is by violating charge conservation via superconductivity. Thus, given a band structure, the Weyl nodes are stable to arbitrary perturbations as long as charge conservation and translational invariance is preserved. Disorder, in general, does not preserve the latter symmetry; however, if the disorder is smooth, many properties of the WSM that rely on the topological nature of the band structure should survive. In contrast, Dirac nodes in graphene can be destroyed individually by breaking lattice point group symmetries.

The topological stability of the Weyl nodes crucially relies on the intersecting bands being non-degenerate. For degenerate bands, terms that hybridize states within a degenerate subspace can in general gap out the spectrum. Thus, the WSM phase necessarily breaks at least one out of time-reversal and inversion symmetries, as the presence of both will make each state doubly degenerate.

Based on (1.1), each Weyl point in a WSM can be characterized by a *chirality quantum number* χ defined as $\chi = \text{sgn}[\det(v_{ij})]$. The physical significance of the chirality is as follows. An electron living in a Bloch band feels an effective vector potential $\mathbf{A}(\mathbf{k}) = i \langle u(\mathbf{k}) | \nabla_{\mathbf{k}} u(\mathbf{k}) \rangle$ because of spatial variations of the Bloch state $|u(\mathbf{k})\rangle$ within a unit cell. The corresponding field strength $\mathbf{F}(\mathbf{k}) = \nabla_{\mathbf{k}} \times \mathbf{A}(\mathbf{k})$, known as the Berry curvature or the Chern flux, plays the role of a magnetic field corresponding to the vector potential $\mathbf{A}(\mathbf{k})$. It can be shown that $\mathbf{F}(\mathbf{k})$ near a Weyl node of chirality χ satisfies

$$\frac{1}{2\pi} \oint_{FS} \mathbf{F}(\mathbf{k}) \cdot d\mathbf{S}(\mathbf{k}) = \chi \quad (1.2)$$

where the integral is over any Fermi surface enclosing the Weyl node and the area element $d\mathbf{S}(\mathbf{k})$ is defined so as to point away from the occupied states. Since $\mathbf{F}(\mathbf{k})$ acts like a magnetic field in momentum space, (1.2) suggests that a Weyl node acts like a magnetic monopole in momentum space whose magnetic charge equals its chirality. Equivalently, a Fermi surface surrounding the Weyl node is topologically non-trivial; it has a Chern number, defined as the Berry curvature integrated over the surface as in (1.2), of χ ($-\chi$) for an electron (a hole) Fermi surface.

Nielsen and Ninomiya [28, 26] showed that the total magnetic charge in a band structure must be zero, which implies that the total number of Weyl nodes must be even, with half of each chirality. The argument is simple and runs as follows. Each 2D slice in momentum space that does not contain any Weyl nodes can be thought of as a Chern insulator. Since Weyl nodes emit Chern flux, the Chern number changes by χ as one sweeps the slices past a Weyl node of chirality χ . Clearly, the Chern numbers of slices will be periodic across the Brillouin zone if and only if there are as many Weyl nodes of chirality χ as there are of chirality $-\chi$. Such a notion of chirality does not exist for graphene or the surface states of topological insulators, which also consist of 2D Dirac nodes, because the Berry phase around a Fermi surface is π which is indistinguishable from $-\pi$.

The fact that each Weyl node is chiral and radiates Chern flux leads to another marvelous phenomenon absent in two dimensions – the *chiral anomaly*. The statement is as follows: suppose the universe (or, for condensed matter

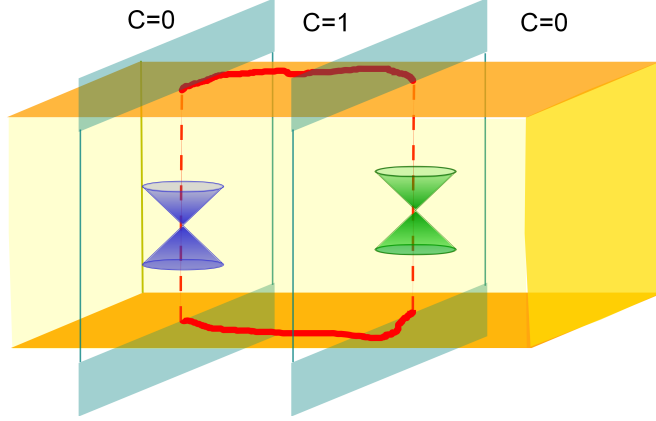


Figure 1.1: Weyl semimetal with a pair of Weyl nodes of opposite chirality (denoted by different colors green and blue) in a slab geometry. The surface has unusual Fermi arc states (shown by red curves) that connect the projections of the Weyl points on the surface. C is the Chern number of the 2D insulator at fixed momentum along the line joining the Weyl nodes. The Fermi arcs are nothing but the gapless edge states of the Chern insulators strung together.

purposes, the band structure) consisted only of Weyl electrons of chirality χ and none of chirality $-\chi$. Then, the electromagnetic current j_χ^μ of these electrons in the presence of electromagnetic fields \mathbf{E} and \mathbf{B} would satisfy ($e > 0$ is the unit electric charge and \hbar is the reduced Planck's constant)

$$\partial_\mu j_\chi^\mu = -\chi \frac{e^3}{4\pi^2 \hbar^2} \mathbf{E} \cdot \mathbf{B} \quad (1.3)$$

i.e., charge would not be conserved! (1.3) can equivalently be written in terms of the electromagnetic fields strength $F_{\mu\nu} = \partial_\mu A_\nu - \partial_\nu A_\mu$, where A_μ is the vector potential, as

$$\partial_\mu j_\chi^\mu = -\chi \frac{e^3}{32\pi^2 \hbar^2} \epsilon^{\mu\nu\rho\lambda} F_{\mu\nu} F_{\rho\lambda} \quad (1.4)$$

where $\epsilon^{\mu\nu\rho\lambda}$ is the antisymmetric tensor. (1.3) and (1.4) seem absurd; however, they makes sense instantly when one recalls that in reality, Weyl nodes always come in pairs of opposite chiralities and the total current $j_+^\mu + j_-^\mu$ is therefore conserved. In fact, the requirement of current conservation is an equally good argument for why the total chirality of the Weyl nodes must vanish. Classically, currents are always conserved no matter what the dispersion. Thus, (1.3) is a purely quantum phenomenon and is an upshot of the path integral for Weyl fermions coupled to an electromagnetic field not being invariant under separate gauge transformations on left-handed and right-handed Weyl fermions, even though the action is. This will be explained in more detail in Sec. 4.

The purpose of this brief review is to recap some of the strange transport phenomena associated with the chiral anomaly in WSMS that have been discussed in the literature so far. The field is mushrooming, so we make no attempt to be exhaustive. Instead, we describe results that are relatively simple, experiment-friendly and *firsts*, to the best of our knowledge. This is an introductory review targeted mainly towards readers new to the subject. Thus, the results are sketched rather than expounded, and readers interested in further details of any result are encouraged to follow up by consulting the original work.

Before embarking on the review, we skim over another striking feature of WSMS – surface states known as *Fermi arcs*. Although this review does not focus on the Fermi arcs, they are such a unique and remarkable characteristic of WSMS that it would be grossly unfair to review WSMS without mentioning Fermi arcs.

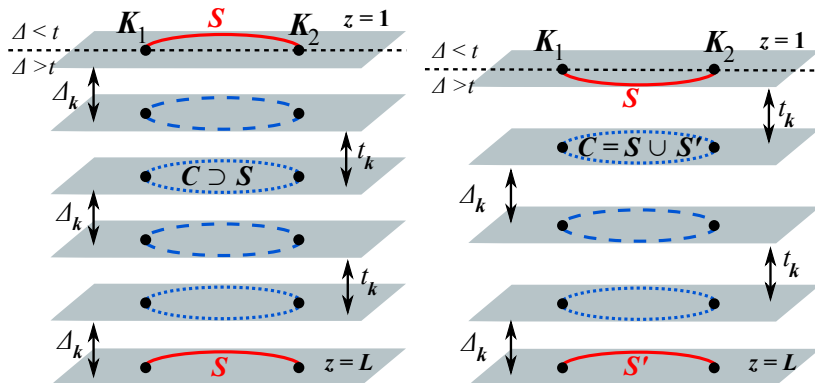


Figure 1.2: Fermi arcs as the residual states of the process of gapping out a stack of 2D Fermi surfaces with momentum-dependent interlayer tunneling. Dotted (dashed) blue curves C represent 2D electron (hole) Fermi surfaces, solid red lines on the end layers labeled S or S' denote Fermi arcs, and Δ_k and t_k are momentum-dependent interlayer hopping amplitudes whose relative magnitudes change at the black dots \mathbf{K}_1 and \mathbf{K}_2 as one moves along the Fermi surface in any layer. Changing the boundary conditions in the left figure by peeling off the topmost layer gives the right figure, which has a different Fermi arc structure. (Hosur [17])

Topological band structures are invariably endowed with topologically protected surface states, and WSMs are no exception. The Fermi surface of a WSM on a slab consists of unusual states known as Fermi arcs. These are essentially a 2D Fermi surface; however, part of this Fermi surface is glued to the top surface and the other, to the bottom. On each surface, Fermi arcs connect the projections of the bulk Weyl nodes of opposite chiralities onto the surface, as shown in Figure 1.1 for the case of two Weyl nodes. A simple way to understand the presence of Fermi arcs is by recalling that momentum space slices not containing Weyl nodes are Chern insulators whose Chern numbers change by unity as one sweeps the slices past a Weyl node. Thus, if the slices far away from the nodes have a Chern number of 0, i.e., the insulators are trivial, the slices between the Weyl nodes are all Chern insulators with unit Chern number. The Fermi arcs, then, are simply the edge states of these insulators. Once WSMs with clean enough surfaces are found, the Fermi arcs should be observable in routine photoemission experiments.

Alternately, Fermi arcs can also be understood as the states left behind by gapping out a stack of 2D Fermi surfaces by interlayer tunneling in a chiral fashion (Hosur [17]). In particular, consider a toy model consisting of a stack of alternating electron and hole Fermi surfaces. For short-ranged interlayer tunneling, each point on each Fermi surface can hybridize in two ways – either with a state in the layer above or with a state in the layer below. If the interlayer tunneling is momentum dependent, such that the preferred hybridization is different for different parts of the Fermi surface, then the points at which the hybridization preference changes become Weyl nodes in the bulk while the end layers have leftover segments that do not have partners to hybridize with and survive as the Fermi arcs. This is shown in Fig 1.2. In this picture, the topological nature of the Fermi arcs is not apparent; however, the way they connect projections of Weyl nodes on the surface becomes transparent. This is in contrast to the previous description of Fermi arcs, in which figuring out what boundary conditions correspond to what connectivity for the Fermi arcs is a highly non-trivial task. The layering picture gives a systematic way to generate Fermi arcs of the desired shape and connectivity, thus facilitating theoretical studies of Fermi arcs significantly.

The rest of the review is organized as follows. We begin by recapping electric transport in WSMs, which characterizes the linear dispersion and not the chiral anomaly *per se*, in Sec. 2. This is followed by an intuitive explanation for the anomaly in Sec. 3. A more formal derivation of the anomaly ensues in Sec. 4, and is succeeded by a description of several simple but striking transport experiments that can potentially serve as signatures of the anomaly in Sec. 5. We conclude with a discussion of the systems in which WSMs have been predicted and the promise the field of WSMs and gapless topological phases holds.

2. Electric transport – bad metal or bad insulator?

The optical conductivity of metals is characterized by a zero frequency Drude peak, whose width is determined by the dominant current relaxation process, in the real, longitudinal part. The Drude peak appears because a metal has gapless excitations which carry current and generically, have non-zero total momentum of the electrons. In the DC limit, relaxation from a current-carrying state to the ground state typically involves electrons scattering off of impurities or, at finite temperatures, interactions with phonons. Each scattering processes produces its own characteristic temperature (T) dependence – the disorder dependent DC conductivity is T independent as long as the impurities are dilute and static, while the rate of inelastic scattering off of phonons grows rapidly with temperature, giving rise to a T^5 dependence of the DC resistivity. Importantly, both these processes, besides relaxing the current, relax the total electron momentum as well. On the other hand, electron-electron interactions conserve momentum and cannot contribute to the conductivity.

Band insulators, on the other hand, have a vanishing DC conductivity simply because they have a band gap, but show a bump in the optical conductivity when the frequency becomes large enough to excite electrons across the gap. A similar bump occurs in the temperature dependence as well when electrons can be excited across the gap thermally. Weak disorder does not change either behavior significantly.

How do WSMs behave? They obviously must rank somewhere between metals and insulators. But are they better thought of as conductors with a vanishingly small density of states at the Fermi level, or as insulators with a vanishing band gap? This question was addressed recently, in the continuum limit (Hosur et al. [18], Burkov et al. [4]) as well as using a lattice model with eight Weyl nodes (Rosenstein and Lewkowicz [30]).

Hosur et al. [18] showed that WSMs, like graphene (Fritz et al. [9]) and 3D Dirac semimetals (Goswami and Chakravarty [12]), actually exhibit a phenomenon that neither metals nor insulators do – DC transport driven by Coulomb interactions between electrons alone, even in a clean system. This is because all these systems possess a particle-hole symmetry about the charge neutrality points, at least to linear order in deviations from these points in momentum space. As a result, there exist current carrying states consisting of electrons and holes moving in opposite directions with equal and opposite momenta. Since the total momentum is zero, Coulomb interactions can indeed relax these states. A quantum Boltzmann calculation gives the DC conductivity at temperature T

$$\sigma_{dc}(T) = \frac{e^2}{h} \frac{k_B T}{\hbar v_F(T)} \frac{1.8}{\alpha_T^2 \log \alpha_T^{-1}} \quad (2.1)$$

where $v_F(T)$ and α_T are the Fermi velocity and fine structure constant renormalized (logarithmically) to energy $k_B T$. (2.1) can be understood within a picture of thermally excited electrons diffusively, as follows. Einstein's relation $\sigma_{dc}(T) = e^2 D(T) \frac{dn(T)}{d\mu}$ expresses σ_{dc} in terms of the density of states at energy $k_B T$, $\frac{dn(T)}{d\mu} \sim \frac{(k_B T)^2}{(\hbar v_F)^3}$, and the diffusion constant $D(T) = v_F^2 \tau(T)$, where $\tau(T)$ is the temperature dependent transport lifetime. Now, the scattering cross-section for Coulomb interactions must be proportional to α^2 because scattering matrix elements are proportional to α . Since T is the only energy scale in the problem, $\tau^{-1}(T) \sim \alpha^2 T$ on dimensional grounds. This immediately gives (2.1) upto logarithmic factors. This behavior has already been seen approximately in the pyrochlore iridates $Y_2\text{Ir}_2\text{O}_7$ (Yanagishima and Maeno [44]), $\text{Eu}_2\text{Ir}_2\text{O}_7$ under pressure (Tafti et al. [32]) and $\text{Nd}_2\text{Ir}_{1-x}\text{Rh}_x\text{O}_7$ ($x \approx 0.02-0.05$) (Ueda et al. [34]), all of which are candidate WSMs.

On the other hand, non-interacting WSMs with chemical potential disorder act like bad metals in some of their transport properties (Hosur et al. [18], Burkov et al. [4], Burkov and Balents [3]). Fig 2.1 shows the temperature and frequency dependence of the optical conductivity of disordered WSMs. Like metals, it has a Drude peak whose height is set by the disorder strength. However, the width of the peak goes as T^2 , unlike metals where the peak width has a weaker dependence – \sqrt{T} – on temperature. Thus, the conductivity at small non-zero frequency falls faster as the temperature is lowered in WSMs as compared to ordinary metals. At high frequencies, the behavior is entirely different. At $\hbar\omega \gg k_B T$, the conductivity grows linearly with the frequency: $\sigma_{xx}(\omega) = \frac{e^2}{12h} \frac{\omega}{v_F}$ per Weyl

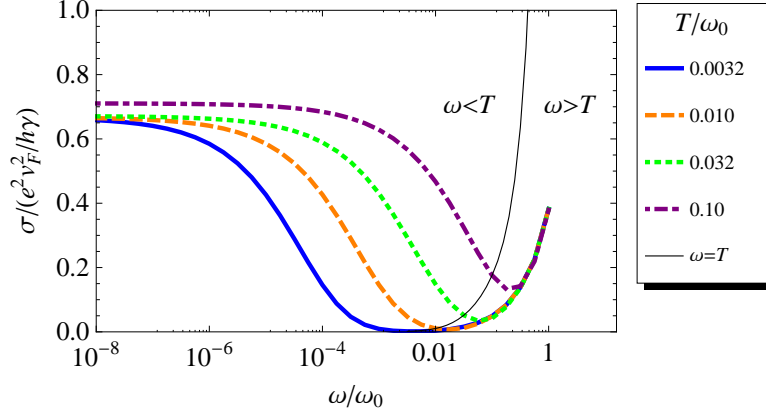


Figure 2.1: Linear-log plot of the optical conductivity of a WSM with Gaussian disorder computed within a Born approximation. The disorder strength is characterized by γ (or $\omega_0 = 2\pi v_F^3/\gamma$). (Hosur et al. [18])

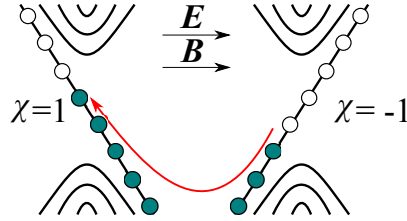


Figure 3.1: Charge pumping between Weyl nodes in parallel electric and magnetic fields in the quantum limit. Each point in the dispersions is a Landau level. Filled (empty) circles denote occupied (unoccupied) states. Only occupation of the chiral zeroth Landau levels are shown because they are the only ones that participate in the pumping.

node. This is expected from dimensional analysis since the only physical energy scale under these circumstances is the frequency. Importantly, such behavior is unparalleled in metals or insulators.

In summary, WSMs are neither metallic nor insulating in most of their electric transport properties. However, if one is forced to put a finger on which of the two more common phases they behave like, (bad) ‘metals’ is more accurate than (bad) ‘insulators’.

3. The chiral anomaly – poor man’s approach

We now turn to the main focus of this review – the chiral anomaly and related anomalous magnetotransport. This is where the story really starts to get fascinating and WSMs start displaying a slew of exotic properties unheard of in conventional electronic phases. To start off, we present a quick caricaturistic derivation of the anomaly to give the reader a feel for the microscopic physics that is at play here.

In a magnetic field \mathbf{B} , the spectrum of the Hamiltonian for a single Weyl node consists of Landau levels of degeneracy $g = \frac{BA_{\perp}}{h/e}$, where A_{\perp} is the cross-section transverse to \mathbf{B} , dispersing along \mathbf{B} . Crucially, the zeroth

Landau disperses only one way, the direction of dispersion depending on the chirality of the Weyl node.

$$\begin{aligned}\epsilon_n &= v_F \text{sign}(n) \sqrt{2\hbar|n|eB + (\hbar\mathbf{k} \cdot \hat{\mathbf{B}})^2}, \quad n = \pm 1, \pm 2, \dots \\ \epsilon_0 &= -\chi \hbar v_F \mathbf{k} \cdot \hat{\mathbf{B}}\end{aligned}\tag{3.1}$$

Suppose the temperature and the chemical potential are much smaller than $v_F \sqrt{\hbar e B}$. Then, only the zeroth Landau level is relevant for the low energy physics and we are in the so-called “quantum limit”. If an electric field \mathbf{E} is now applied in the same direction as \mathbf{B} , all the states move along the field according to $\hbar \dot{\mathbf{k}} = -e\mathbf{E}$. The key point is that the zeroth Landau level is chiral, i.e., it disperses only one way for each Weyl node. Therefore, motion of the states along \mathbf{E} corresponds to electrons disappearing from right-moving band and reappearing in the left-moving one, as depicted in Fig 3.1. In other words, the charge in each of the g chiral Landau bands is non-conserved, and each of these bands exhibits a *1D chiral anomaly*, given by $\partial Q_\chi^{1D}/\partial t = e\chi L_B |\dot{\mathbf{k}}|/2\pi = -e^2 \chi L_B |\mathbf{E}|/h$, where L_B is the system size in the direction of \mathbf{B} . Multiplying by g gives the 3D result

$$\frac{\partial Q_\chi^{3D}}{\partial t} = g \frac{\partial Q_\chi^{1D}}{\partial t} = -V \frac{e^3}{4\pi^2 \hbar^2} \mathbf{E} \cdot \mathbf{B}\tag{3.2}$$

where $V = A_\perp L_B$ is the system volume. This is the same as (1.3) in the special case of a translationally invariant system, in which the current due to a single Weyl node is divergence free $\nabla \cdot \mathbf{j}_\chi = 0$. The above “quantum limit” derivation is the simplest and most intuitive way to understand (1.3). The result, however, is not restricted to quantum limit. Indeed, charge pumping between Weyl nodes of opposite chiralities was recently shown in a purely semiclassical formalism as well, by Son and Spivak [31].

4. The chiral anomaly – general derivation

A more general field theoretic to understand the chiral anomaly is by making the following observation. Just as there exists a quantum Hall state in two dimensions which carries chiral 1D gapless edge states, there is an analogous 4D state whose surface has chiral 3D gapless edge states with opposite chiralities localized on opposite surfaces (Zhang and Hu [47]). Now, in the absence of any internode scattering, the two nodes of a WSM can be thought of as such surface states, and the anomaly must emerge from the surface theory of the hypothetical 4D quantum Hall state.

The bulk effective theory for electromagnetic fields for the 4D state contains the topological third Chern-Simons term:

$$S_{QH}^{4D} = \int d^5x \left(\frac{e^3}{8\pi^2 \hbar^2} \epsilon^{\mu\nu\rho\sigma\lambda} A_\mu \partial_\nu A_\rho \partial_\sigma A_\lambda + A_\mu j^\mu \right)\tag{4.1}$$

just as that in a 2D quantum Hall state contains the second Chern Simons term¹. S_{QH}^{4D} is well-defined in the bulk, but it violates gauge invariance at the boundary. As a consequence, some of the gauge degrees of freedom become physical and survive as gapless fermionic states glued to the boundary, viz., the Weyl nodes. To see the anomaly

¹It also contains the usual Maxwell term $S_{Max} \sim \int d^5x F_{\mu\nu} F^{\mu\nu}$. As we shall see in a moment, the anomaly stems from broken gauge invariance of the Chern-Simons action at the boundary. S_{Max} is gauge invariant everywhere, so it does not contribute to the anomalous physics and will thus be dropped. An important difference between 2+1D and 4+1D Chern-Simons theories is that the former contains only one derivative and hence, dominates the Maxwell term in the long-distance physics, whereas the latter has two derivatives and competes with the Maxwell term even at long distances.

in this picture, let us generalize the procedure outlined by Maeda [23] in two dimensions and insert a step function $\Theta(x_4)$ to simulate a surface normal to x_4 , the imaginary dimension, into the action:

$$\tilde{S}_{QH}^{4D} = \int d^5x \left(\frac{e^3}{8\pi^2\hbar^2} \Theta(x_4) \epsilon^{\mu\nu\rho\sigma\lambda} A_\mu \partial_\nu A_\rho \partial_\sigma A_\lambda + A_\mu j^\mu \right). \quad (4.2)$$

The equation of motion $\frac{\partial \mathcal{L}}{\partial A_\mu} = \partial_\nu \left(\frac{\partial \mathcal{L}}{\partial_\nu A_\mu} \right)$ now contains an extra term on the right hand side proportional to $\partial_4 \Theta(x_4) = \delta(x_4)$, which is clearly localized on the boundary. After an integration by parts, the boundary current can be shown to satisfy (1.3). This is the essence of the Callan-Harvey mechanism, which is well-known in the context of the 2D integer quantum Hall effect but is equally well applicable here. In this picture, the charge carried by the boundary states is not conserved because it can always vanish into the bulk and reappear on a different boundary.

A third approach to understanding the chiral anomaly entails encapsulating the anomaly in the action itself rather than computing the chiral current. The advantage of such an approach is that once the effective action for the electromagnetic fields is known, physical transport properties can be derived immediately. Below, we sketch one such technique known as the Fujikawa rotation technique (see, for example, Hosur et al. [16]) for deriving such an action. The technique transforms the action of a WSM with two Weyl nodes into a massless Dirac action supplemented by a topological θ -term. The latter is a consequence of the anomaly and is absent in an ordinary Dirac action. This was the approach adopted in some recent works (Zyuzin and Burkov [49], Goswami and Tewari [13], Chen et al. [7]).

Consider the continuum Euclidean action

$$S_W = \int d^4x \bar{\psi} \gamma^\mu (\hbar i \partial_\mu - e A_\mu - b_\mu \gamma^5) \psi \quad (4.3)$$

where ψ and $\bar{\psi} = \psi^\dagger \gamma^0$ are Grassman spinor fields, b_μ is a constant 4-vector, γ^μ , $\mu = 0 \dots 3$ are the standard 4×4 Dirac matrices and $\gamma^5 = i\gamma^0\gamma^1\gamma^2\gamma^3$ is the chirality or ‘‘handedness’’ operator. In other words, right-handed and left-handed Weyl nodes correspond to eigenstates of γ^5 with eigenvalues $+1$ and -1 , respectively. All the five γ -matrices anti-commute with one another. S_W describes a Weyl metal (not a WSM, unless $b_0 = 0$) with two Weyl nodes separated in momentum space by $\mathbf{b} = (b_x, b_y, b_z)$ and in energy by b_0 coupled to the electromagnetic field. S_W is clearly invariant under a chiral gauge transformation

$$\psi \rightarrow e^{-i\theta(x)\gamma^5/2} \psi \text{ or } \psi_\pm \rightarrow e^{\mp i\theta(x)/2} \psi_\pm, \gamma^5 \psi_\pm = \pm \psi_\pm \quad (4.4)$$

which suggests that the chiral current $j_{ch}^\mu = e \bar{\psi} \gamma^\mu \gamma^5 \psi$ is conserved. This is clearly wrong because we know that j_{ch}^μ conservation is violated according to (1.3). What went wrong?

The flaw in the above argument becomes obvious when one realizes that in a real condensed matter system, the right-handed and left-handed Weyl nodes are connected at higher energies, so ψ_+ and ψ_- cannot be gauge transformed separately as in (4.4). In other words, the true action of the system changes under (4.4), and the change comes from the regularization of the theory at high energies.

To compute this change, let us perform such a transformation and see what happens. If we choose $\theta(x) = (2\mathbf{b} \cdot \mathbf{r} - 2b_0 t)/\hbar$, b_μ gets eliminated from S_W , leaving behind a massless Dirac action $S_D = \int d^4x \bar{\psi} i \gamma^\mu (\hbar \partial_\mu + ie A_\mu) \psi$ in which both the chiral current j_{ch}^μ as well as the total current $j^\mu = e \bar{\psi} \gamma^\mu \psi$ are truly conserved. However, the measure of the path integral $\mathcal{Z} = \int \mathcal{D}\psi \mathcal{D}\bar{\psi} e^{-S_W[\psi, \bar{\psi}]}$ is not invariant under (4.4), which signals an anomaly. More precisely, the Jacobian of the transformation is non-trivial and can be interpreted as an additional term in the Dirac action:

$$\mathcal{D}\psi \mathcal{D}\bar{\psi} \rightarrow \mathcal{D}\psi \mathcal{D}\bar{\psi} \det \left[e^{i\theta(x)\gamma^5} \right] \equiv \mathcal{D}\psi \mathcal{D}\bar{\psi} e^{-S_\theta/\hbar} \implies S_\theta = -i\hbar \text{Tr} \left[\theta(x) \gamma^5 \right] \quad (4.5)$$

thus giving $S_W = S_D + S_\theta$.² Information about the violation of chiral gauge invariance at high energies is now expected to be contained in S_θ .

The meaning of the trace in (4.5) is highly subtle, and it is not a simple trace of the matrix γ^5 multiplied by a scalar function $\theta(x)$. If it were, S_θ would vanish because γ^5 is traceless. Rather, it represents a sum over a complete basis of fermionic states with suitable regularization. A natural basis choice is the eigenstates of the Dirac operator $\mathcal{D} = \gamma^\mu(\hbar\partial_\mu + ieA_\mu)$; a regularization method traditionally used in particle physics literature is the heat kernel regularization, which exponentially suppresses states at high energy. Thus,

$$\begin{aligned} \text{Tr} [\theta(x)\gamma^5] &= \lim_{M \rightarrow \infty} \int d^4x \sum_n \phi_n^*(x) e^{-\epsilon_n^2/M^2} \theta(x) \gamma^5 \phi_n(x) \\ &= \lim_{M \rightarrow \infty} \int d^4x \sum_n \phi_n^*(x) e^{-\mathcal{D}^2/M^2} \theta(x) \gamma^5 \phi_n(x) \end{aligned} \quad (4.6)$$

where

$$\begin{aligned} \mathcal{D}\phi_n(x) &= \epsilon_n \phi_n(x) \\ \int d^4x \phi_n^*(x) \phi_m(x) &= \delta_{nm} \quad , \quad \sum_n \phi_n^*(x) \phi_n(y) = \delta(x-y) \end{aligned} \quad (4.7)$$

The right hand side in (4.6) can be evaluated by Fourier transforming to momentum space and using the completeness relations in (4.7) (See Zyuzin and Burkov [49] or Goswami and Tewari [13] for details). The result is S_θ in terms of the electromagnetic fields:

$$S_\theta = \frac{ie^2}{32\pi^2\hbar^2} \int d^4x \theta(x) \epsilon^{\mu\nu\rho\lambda} F_{\mu\nu} F_{\rho\lambda} = \frac{ie^2}{4\pi^2\hbar^2} \int d^4x \theta(\mathbf{r}, t) \mathbf{E} \cdot \mathbf{B} \quad (4.8)$$

Note that electromagnetic fields entered the derivation via the Dirac operator \mathcal{D} in the regularization step in (4.5). One could choose a different regularization; a natural choice for condensed matter systems would be to add non-linear terms to the dispersion. However, electromagnetic fields will still enter the derivation via minimal coupling and the final result for S_θ should be the same. In fact, it turns out that some sort of regularization is unavoidable, because the right hand side of (4.5) without it is the difference of two divergent terms and is thus ill-defined. We had earlier anticipated precisely this fact – the chiral anomaly is nothing but a shadow of the violation of chiral symmetry at high energies in the low energy physics, and must originate in the high energy regularization of the theory.

(4.8) is eerily similar to the magnetoelectric term that appears in the action of a 3D topological insulator. There is an important difference, however. In topological insulators, $\theta(\mathbf{r}, t)$ takes a constant value $\theta = \pi$ whereas here it is a spacetime dependent scalar field. This subtle difference immediately leads to novel topological properties in WSMs, some of which we discuss below. Moreover, if translational symmetry is broken and the Weyl nodes are gapped out by charge density wave order at the wavevector that connects them, it can be shown that $\theta(\mathbf{r}, t)$ survives as phase degree freedom of the density wave, which is the Goldstone mode of the translational symmetry breaking process (Wang and Zhang [39]).

²Strictly speaking, the gauge transformation (4.4) to remove b_μ from S_W must be done in a series of infinitesimal steps. However, the contribution to S_θ from each step happens to be the same, so we are justified in doing the transformation at once.

5. Anomaly induced magnetotransport

Having understood the basic idea of the chiral anomaly, we now describe several transport signatures of this effect.

5.1. Negative magnetoresistance

One of the first transport signatures of the chiral anomaly was pointed out more than 30 years ago by Nielsen and Ninomiya (Nielsen and Ninomiya [27]). They noted that since Weyl nodes are separated in momentum space, any charge imbalance created between them by an $\mathbf{E} \cdot \mathbf{B}$ field or otherwise requires large momentum scattering processes in order to relax. In a sufficiently clean system, such processes are relatively weak, resulting in a large relaxation time. An immediate consequence of this is that the longitudinal conductivity along an applied magnetic field, which is proportional to the relaxation time, is extremely large. Moreover, a WSM in a magnetic field reduces to a large number – equal to the degeneracy of the Landau levels – of decoupled 1D chains dispersing along the field as show in Fig 3.1. Therefore, the conductivity is proportional to the magnetic field or, equivalently, the resistivity decreases with increasing magnetic field. This phenomenon is termed as *negative magnetoresistance*.

Being one of the simplest signatures of the anomaly, negative magnetoresistance has also been the first one to have been observed experimentally (Kim et al. [20]). The material on which the experiment was performed was $\text{Bi}_{0.97}\text{Sb}_{0.03}$. Bi (Sb) is known to have topologically trivial (non-trivial) valence bands in the sense of a 3D strong topological insulator. Therefore, it is possible to fine tune $\text{Bi}_{1-x}\text{Sb}_x$ to the critical point separating the two phases (Fu and Kane [10], Murakami [25], Hsieh et al. [19]). The critical point has a single Dirac node in its bands structure. Kim et al. [20] applied a magnetic field at the critical point, which not only created Landau levels but also split the Dirac node into two Weyl nodes. The magnetoconductivity was subsequently measured, the main result of which for our purposes is shown in Fig 5.1. Beyond a very small field strength, there is a clear negative contribution to the resistivity that is enormous for longitudinal fields but very small for transverse ones. The positive contributions to the resistivity at very small fields are attributed to weak anti-localization of the Dirac node at the critical point, while those at very large fields are probably because the large number of 1D modes dispersing along the field become independent 1D systems and can be easily localized.

5.2. Anomalous Hall and chiral magnetic effects

The next set of effects we shall discuss are the anomalous Hall effect (AHE) and the chiral magnetic effect (CME). Although the effects appear to be quite different, their derivation using the field theory outlined in Sec 4 shows that they are simply related by Lorentz transformation and are conveniently discussed together.

By carrying out an integration by parts in (4.8), dropping boundary terms and Wick rotating to real time, S_θ can be written as

$$S_\theta = -\frac{e^2}{8\pi^2\hbar} \int dt d\mathbf{r} \partial_\mu \theta \epsilon^{\mu\nu\rho\lambda} A_\nu \partial_\rho A_\lambda \quad (5.1)$$

Varying with respect to the vector potential gives the currents $j_\nu = \frac{e^2}{4\pi^2\hbar} \partial_\mu \theta \epsilon^{\mu\nu\rho\lambda} \partial_\rho A_\lambda$. Recalling that $\theta(x) = (2\mathbf{b} \cdot \mathbf{r} - 2b_0 t)/\hbar$ gives

$$\mathbf{j} = \frac{e^2}{2\pi^2\hbar^2} \mathbf{b} \times \mathbf{E} + \frac{e^2}{2\pi^2\hbar^2} b_0 \mathbf{B} \quad (5.2)$$

The first term in (5.2) is the AHE in the plane perpendicular to \mathbf{b} . This can be understood based on the picture for Fermi arcs presented in the introduction. We quickly repeat the argument here: each 2D slice of momentum space perpendicular to \mathbf{b} can be thought of as an insulator with a gap that depends on the momentum parallel to \mathbf{b} . Since Weyl nodes are sources of unit Chern flux with a sign proportional to their chirality, the slices between $\mathbf{k} = -\mathbf{b}/2$ and $\mathbf{k} = \mathbf{b}/2$ are Chern insulators with unit Chern number, while those outside this region are

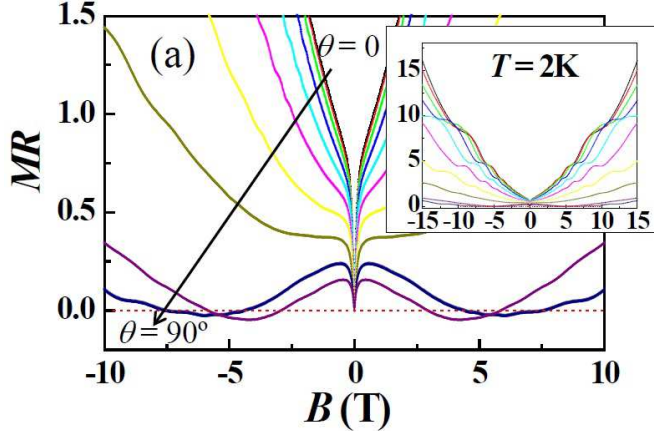


Figure 5.1: Magnetoconductance (MR) of $\text{Bi}_{1-x}\text{Sb}_x$ tuned to a quantum critical point as a function of the magnetic field B . $\theta = 90^\circ$ ($\theta = 0$) corresponds to longitudinal (transverse) magnetoconductance. B seemingly splits the Dirac node into two Weyl nodes in addition to creating Landau levels. The initial rise in MR at very small fields is attributed to weak antilocalization of the Dirac node, while the chiral anomaly is responsible for the subsequent flattening or decrease in it, as explained in Sec 5.1. The effect of the anomaly is clearly more pronounced for longitudinal configurations. The upturn at very large fields is probably due to localization of the 1D modes that constitute the quantum limit picture described in the text. (Figure from Kim et al. [20])

trivial insulators. Each of these Chern insulators has unit Hall conductivity and as a result, the WSM has a Hall conductivity proportional to \mathbf{b} . This result has been derived in several recent works, both in lattice as well as in continuum models (Chen et al. [7], Xu et al. [43], Goswami and Tewari [13], Yang et al. [45], Vafeek and Vishwanath [35], Burkov and Balents [3], Zyuzin and Burkov [49]), and has been accepted unanimously.

The second term in (5.2), known as the chiral magnetic effect (CME), is subtler, and has created some controversy. It predicts an equilibrium dissipationless current parallel to the magnetic field if the two Weyl nodes are at different energies. Zhou et al. [48] obtained the same result in a semiclassical limit. The CME is (deceptively, as we will see) easy to understand in the DC continuum limit: if the Weyl nodes are at different energies, the chiral zeroth Landau level states from the two nodes will have different occupations and their currents will not cancel each other.

However, as pointed out by Vazifeh and Franz [36], this seems to be at odds with some basic results of band theory. In particular, a DC magnetic field reduces the 3D WSM to a highly degenerate 1D system dispersing along the field. The total current DC along the field is

$$j_B = \int_{k_L}^{k_R} g \frac{\partial \epsilon}{\partial k} dk = g(\epsilon_R - \epsilon_L) \quad (5.3)$$

where k_L and k_R are the momenta of the Fermi points of the 1D system, $g = \frac{BA}{h/e}$ is the Landau level degeneracy and $\epsilon(k)$ is the 1D dispersion. At equilibrium, $\epsilon_R = \epsilon_L$, which implies j_B vanishes. Vazifeh and Franz [36] argued that the CME was an artifact of linearizing the dispersion near the Weyl nodes, and is in fact absent in a full lattice model. The CME seems wrong for another reason too. If a state carries a net DC current \mathbf{J} , then Ohmic power $\sim \mathbf{J} \cdot \mathbf{E}$ can be supplied to or extracted from it by applying an appropriate electric field \mathbf{E} . But a ground state is already the lowest energy state, so it is not possible to extract energy from it. Therefore it cannot carry a DC current (Basar et al. [2]).

Soon after, though, this claim was countered by Chen et al. [7] who showed, by rederiving the CME in a lattice model, that while the CME is unambiguously non-zero at finite momentum \mathbf{q} and frequency ω , its DC limit depends

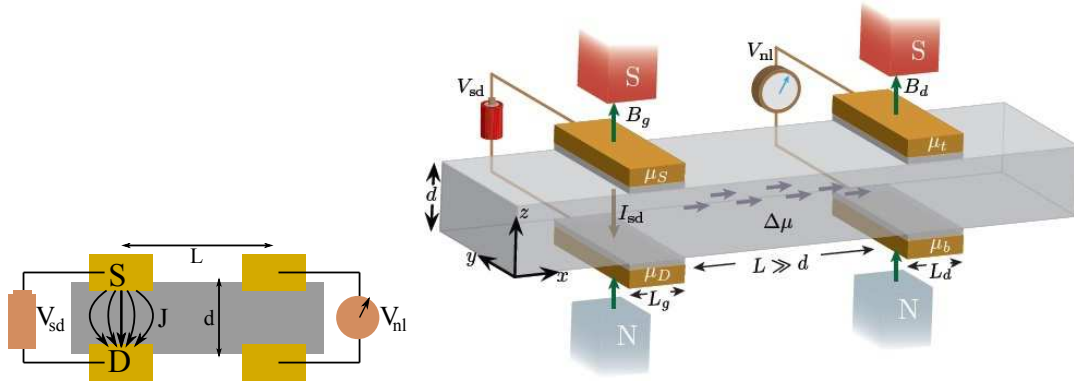


Figure 5.2: (Left) A current J driven between the source (S) and drain (D) leads in an ordinary piece of metal takes the path indicated by the arrows inside the sample. The Ohmic voltage between the top and the bottom surfaces decays over the length scale of the sample thickness d as one moves away from the injection region, so that $V_{nl} \sim V_{sd}e^{-L/d}$. (Right) In a WSM, a local magnetic field B_g along the injected current generates a valley imbalance as a result of the anomaly. This imbalance diffuses slowly if the intervalley scattering processes are weak, and can be detected far away from the injection region by a probe magnetic field B_p which converts it into an electric field. (Right figure from Parameswaran et al. [29])

on the order of the limits $\omega \rightarrow 0$ and $\mathbf{q} \rightarrow 0$. If $\omega \rightarrow 0$ is taken first, one obtains a static system in which the electrons are always in equilibrium and the CME vanishes as predicted by Ref. Vazifeh and Franz [36]. However, the effect survives if the $\mathbf{q} \rightarrow 0$ limit is evaluated first and is precisely that predicted by 5.2. In this case, the electrons are not in equilibrium except *at the limit*, and neither the band theory argument nor the Ohmic dissipation argument presented above applies.

5.3. Non-local transport

Consider a 3D piece of ordinary metal with four contacts attached to it, as shown in Fig 5.2 (left). The two contacts on the left, labeled source (S) and drain (D) inject a current J through the sample, whose typical path is indicated by the arrows connecting the S and the D leads. As one moves away from S and D , the voltage drop between the upper and lower surfaces falls because smaller and smaller segments of the current lines are encountered by a path that goes vertically from the top to the bottom surface. In particular, it can be shown that in the “quantum limit” where the mean free path is limited only by the contacts, the nonlocal voltage drop V_{nl} decays on the scale of the sample thickness d .

Parameswaran et al. [29] showed that the situation in WSMs in the presence of local magnetic fields is strikingly different. As a consequence of the anomaly, a local magnetic field applied parallel to the injected current generates an imbalance in the occupation numbers of the two Weyl nodes locally. This imbalance diffuses over a length scale l determined by the rate of internode scattering processes and hence, can be quite large – even larger than the sample thickness d . Thus, at distances $L \sim l \gg d$ there are no Ohmic voltages but there exists a *valley* imbalance, borrowing nomenclature from semiconductor physics. Detecting the valley imbalance is challenging, however, because it does not couple to electric fields. The anomaly comes to the rescue, and the last piece of the puzzle entails applying a local probe magnetic field. This couples to the valley imbalance and produces a local electric field which can then be measured by conventional methods.

5.4. Chiral gauge anomaly

The final effect we will describe is the response to a chiral gauge field, i.e., a gauge field that has opposite signs for Weyl nodes of opposite chirality. One way to create such a field is by applying appropriate strains, as has been

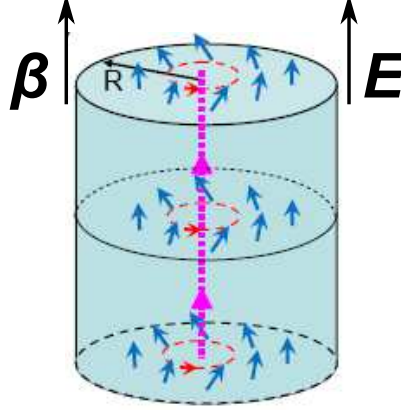


Figure 5.3: A vortex in the magnetization (small blue arrows) results in a chiral magnetic field β along the vortex axis. An electric field in the same direction then generates a one way current moving along the vortex axis. (Liu et al. [21])

done in graphene (Castro Neto et al. [5]) to apply opposite gauge fields to the two Dirac nodes there. More generally, chiral gauge fields can be created in WSMs by exploiting the fact that a general Weyl metal can be created from a Dirac semimetal by breaking time-reversal and inversion symmetries. Then, fluctuations in the perturbations that break these symmetries naturally act like chiral gauge fields.

Liu et al. [21] pointed out that chiral gauge fields in a WSM induce an anomaly not only in the chiral current but also in the total electric current. The argument is simple. Suppose A_μ and a_μ are the electromagnetic and the chiral gauge fields, respectively, and $F_{\mu\nu}$ and $f_{\mu\nu}$ the corresponding field strengths. Then, a Weyl node of chirality χ feels a total gauge field $\mathcal{A}_\mu^\chi = A_\mu + \chi a_\mu$ and hence, suffers from an anomaly $\partial_\mu j_\chi^\mu = -\chi \frac{e^3}{4\pi^2 \hbar^2} \epsilon^{\mu\nu\rho\lambda} \partial_\mu \mathcal{A}_\nu^\chi \partial_\rho \mathcal{A}_\lambda^\chi$ according to (1.4). Consequently, the conservation laws for the chiral current $j_{ch}^\mu = j_+^\mu - j_-^\mu$ and the total current $j^\mu = j_+^\mu + j_-^\mu$ read

$$\partial_\mu j_{ch}^\mu = -\frac{e^3}{16\pi^2 \hbar^2} \epsilon^{\mu\nu\rho\lambda} (F_{\mu\nu} F_{\rho\lambda} + f_{\mu\nu} f_{\rho\lambda}) \quad (5.4)$$

$$\partial_\mu j^\mu = -\frac{e^3}{8\pi^2 \hbar^2} \epsilon^{\mu\nu\rho\lambda} F_{\mu\nu} f_{\rho\lambda} \quad (5.5)$$

(5.4) is the usual chiral anomaly which receives additional contribution from the chiral gauge fields. (5.5), however, states that even the total current is not conserved if both electromagnetic and chiral gauge fields are present. This can be rewritten in terms of the chiral “magnetic field” $\beta = \nabla \times \mathbf{a}$ and chiral “electric field” $\varepsilon = -\nabla a_0 - \frac{\partial \mathbf{a}}{\partial t}$ as

$$\partial_\mu j^\mu = -\frac{e^3}{2\pi^2 \hbar^2} (\beta \cdot \mathbf{E} + \varepsilon \cdot \mathbf{B}) \quad (5.6)$$

If time-reversal symmetry in the system is broken by ferromagnetism, then \mathbf{a} is proportional to the magnetic moment and the chiral magnetic field corresponds to a ferromagnetic vortex. The first term above, then, predicts a chiral current propagating along the vortex axis. In the quantum limit picture of Sec 3, this current is carried by zeroth Landau levels states, which now disperse in the same direction for both Weyl nodes. An immediate question is, how can charge not be conserved in a real system? The answer comes from the realization that unlike A_μ , a_μ is a physical field and must be single valued. Since $a_\mu = 0$ in vacuum, the total flux $\beta = \nabla \times \mathbf{a}$ must vanish in a finite system. Equivalently, the total winding number of all the vortices must be zero. Thus, there are equal numbers

of chiral and antichiral modes so that the total current is, in fact, conserved. These modes are in different spatial regions, so the gauge anomaly (5.5) is still meaningful locally.

The second term is generated by a time-dependent magnetization, and describes charge and current modulations in response to magnetization fluctuations in the presence of \mathbf{B} . In other words, it describes a coupling between plasmons (charge fluctuations) and magnons (magnetic fluctuations), which is not present in ordinary metals or semimetals.

6. Materials realizations

Theorists have occasionally enthused over 3D Dirac (Abrikosov and Beneslavskii [1]) and Weyl (Nielsen and Ninomiya [28, 26, 27]) band structures for decades and it has long been known that the A-phase of superfluid Helium-3 has Weyl fermions (Volovik [37], Meng and Balents [24]). However, interest in them has recently been rekindled by the prediction that some simple electronic systems realize them.

The first materials prediction was in the pyrochlore iridates family – $R_2Ir_2O_7$ – where ‘R’ is a rare earth element (Wan et al. [38], Witczak-Krempa and Kim [42], Chen and Hermele [6]). These candidate WSMs are inversion symmetric but break time-reversal symmetry via a special kind of anti-ferromagnetic ordering – the ‘all-in/all-out’ ordering – in which all the spins on a given tetrahedron point either towards the center or away from it, and the ordering alternates on adjacent tetrahedra. Available transport data on these materials are roughly consistent with linearly dispersing bands (Yanagishima and Maeno [44], Tafti et al. [32], Ueda et al. [34]); however, the evidence is far from conclusive as yet. In its footsteps followed several proposals to engineer WSMs in topological insulators heterostructures. Alternately stacking topological and ferromagnetic insulators was shown to produce inversion symmetric WSMs in a certain parameter regime with Weyl nodes separated along the stacking direction (Burkov and Balents [3]), while replacing the ferromagnetic insulators with trivial, time-reversal symmetric ones and applying an electric field perpendicular to the layers could give time-reversal symmetric WSMs (Halász and Balents [14]). A third option is to magnetically dope a quantum critical point separating a topological and trivial insulator (Cho [8]). An advantage of this realization, as we saw in Sec 5.4, is that magnetization can be used as a handle to dynamically modify the band structure; in return, magnetic textures and fluctuations are endowed with physical properties that uniquely characterize the topological nature of the underlying bands (Liu et al. [21]).

Some closely related phases have been predicted in real materials as well. A ferromagnetic spinel $HgCr_2Se_4$ has been predicted to form a double WSM, i.e., a WSM in which the Weyl nodes have magnetic charge of ± 2 (Xu et al. [43]). Passing light through a cleverly designed photonic crystal gives it a dispersion that can be fine-tuned to have with “Weyl” line nodes, i.e., a pair of non-degenerate bands intersecting along a line (Lu et al. [22]). The surface states of such a crystal has flat bands, implying photon states with zero velocity. Unlike electronic systems, such a band structure can be obtained while preserving time-reversal and inversion symmetries because there is no Kramers degeneracy for photons. Breaking these symmetries reduces the line node to Weyl points. Finally, ab initio calculations have predicted dispersions with degenerate Weyl nodes in β -cristobalite BiO_2 (Young et al. [46]), A_3Bi where $A=Na$ or K (Wang et al. [41]) and Cd_3As_2 (Wang et al. [40]). Whereas the first two are inversion symmetric Dirac semimetals, a combination of broken inversion symmetry and unbroken crystal symmetries in Cd_3As_2 holds Weyl nodes of opposite chiralities degenerate but gives them distinct Fermi velocities.

7. Summary

We have made a humble attempt at introducing Weyl semimetals and recapping the recent theoretical and experimental developments in the transport studies of this phase. The basics of WSMs can be summarized in three main points. These points are interrelated and any one can be deduced from any other.

- The first is the definition itself, that it has a band structure with non-degenerate bands intersecting at arbitrary points in momentum space. An immediate consequence of such band intersections is that Weyl points are topologically robust as long as translational symmetry is present. Moreover, the dispersion in the neighborhood of these points is linear. We reviewed the transport properties contingent on the linear dispersion in Sec 2. There, we stated that unlike metals, WSMs can have a finite DC conductivity driven purely by electron-electron interactions. We concluded the section by stating that WSMs resemble metals more than insulators based on disorder dependent transport.
- The second key feature of WSMs is the chiral anomaly. Weyl nodes can be characterized by a chirality quantum number of ± 1 ; the chiral anomaly says that chiral charge, i.e., the number of quasiparticles around Weyl nodes of fixed chirality, is not conserved in the presence of parallel electric and magnetic fields. In other words, an $\mathbf{E} \cdot \mathbf{B}$ field pumps charge between Weyl nodes of opposite chiralities. We presented two detailed derivations of the anomaly in Sec 4. The first treats Weyl nodes as the surface states of a 4D quantum Hall system. In this picture, the anomaly is understood as charge pumping between opposite surfaces of a topological phase. The second works entirely in three dimensions, and captures the anomaly in a term in the action that supplements the one that gives the Weyl nodes a linear dispersion. In this derivation, it becomes apparent that the anomaly exists because separate gauge transformations on Weyl fermions of opposite chiralities is forbidden by states at higher energies. Once the anomaly was introduced in some detail, we presented several recent theoretical predictions for anomalous transport. These included a negative contribution to magnetoresistance that has nothing to do with weak localization (Sec 5.1), anomalous Hall effect as well as a current along an applied magnetic field (Sec 5.2), extremely slow decay of a voltage in the presence of a magnetic field in the same direction as the voltage (Sec 5.3), and non-conservation of ordinary current due to fluctuations in the background fields that split a Dirac node into Weyl nodes thus giving a WSM (Sec 5.4). We also flashed experimental results on $\text{Bi}_{1-x}\text{Sb}_x$ which shows striking negative magnetoresistance consistent with the chiral anomaly.
- The third key characteristic of WSMs is peculiar surface states known as Fermi arcs. These can either be thought of as the edge states of Chern insulators layered in momentum space, or as the remnants of the process of destroying a stack of electron and hole Fermi surfaces in a chiral fashion. Once suitable materials are found, these states should be easily observable in photoemission experiments.

We wrapped up the review by touching upon several systems in which WSMs have been predicted to occur. So far, these include certain pyrochlore iridates, heterostructures based on topological insulators and systems with Dirac nodes perturbed by suitable symmetries. $\text{Bi}_{0.97}\text{Sb}_{0.03}$ placed in a magnetic field belongs to the last category. Magnetotransport data on it is the best evidence thus far of the WSM phase being realized in a real system. Nonetheless, the naturalness of 3D band crossings and the number of materials predictions that have been made in a short time are compelling indications that the field of WSMs and gapless topological phases is well and truly blossoming.

8. Acknowledgments

We are indebted to Jerome Cayssol for inviting us to write the review. We would like to thank Daniel Bulmash and Ashvin Vishwanath for valuable feedback on the manuscript and the David and Lucile Packard Foundation for financial support.

References

- [1] A. A. Abrikosov and S. D. Beneslavskii. Some properties of gapless semiconductors of the second kind. *Journal of Low Temperature Physics*, 5:141–154, 1971. ISSN 0022-2291. URL <http://dx.doi.org/10.1007/BF00629569>.
- [2] G. Basar, D. E. Kharzeev, and H.-U. Yee. Triangle anomaly in Weyl semi-metals. *ArXiv e-prints*, May 2013.
- [3] A. A. Burkov and L. Balents. Weyl semimetal in a topological insulator multilayer. *Phys. Rev. Lett.*, 107:127205, Sep 2011. doi: 10.1103/PhysRevLett.107.127205.
- [4] A. A. Burkov, M. D. Hook, and Leon Balents. Topological nodal semimetals. *Phys. Rev. B*, 84:235126, Dec 2011. doi: 10.1103/PhysRevB.84.235126.
- [5] A. H. Castro Neto, F. Guinea, N. M. R. Peres, K. S. Novoselov, and A. K. Geim. The electronic properties of graphene. *Rev. Mod. Phys.*, 81:109–162, Jan 2009. doi: 10.1103/RevModPhys.81.109. URL <http://link.aps.org/doi/10.1103/RevModPhys.81.109>.
- [6] Gang Chen and Michael Hermele. Magnetic orders and topological phases from f - d exchange in pyrochlore iridates. *Phys. Rev. B*, 86:235129, Dec 2012. doi: 10.1103/PhysRevB.86.235129. URL <http://link.aps.org/doi/10.1103/PhysRevB.86.235129>.
- [7] Y. Chen, S. Wu, and A. A. Burkov. Axion response in Weyl semimetals. *ArXiv e-prints*, June 2013.
- [8] G. Y. Cho. Possible topological phases of bulk magnetically doped Bi₂Se₃: turning a topological band insulator into the Weyl semimetal. *ArXiv e-prints*, October 2011.
- [9] L. Fritz, J. Schmalian, M. Müller, and S. Sachdev. Quantum critical transport in clean graphene. *Phys. Rev. B*, 78:085416, Aug 2008. doi: 10.1103/PhysRevB.78.085416. URL <http://link.aps.org/doi/10.1103/PhysRevB.78.085416>.
- [10] L. Fu and C. L. Kane. Topological insulators with inversion symmetry. *Phys. Rev. B*, 76(4):045302, 2007. doi: 10.1103/PhysRevB.76.045302.
- [11] A. K. Geim and K. S. Novoselov. The rise of graphene. *Nat. Mater.*, 6(3):183–191, 03 2007.
- [12] P. Goswami and S. Chakravarty. Quantum criticality between topological and band insulators in $3 + 1$ dimensions. *Phys. Rev. Lett.*, 107:196803, Nov 2011. doi: 10.1103/PhysRevLett.107.196803. URL <http://link.aps.org/doi/10.1103/PhysRevLett.107.196803>.
- [13] P. Goswami and S. Tewari. Axion field theory and anomalous non-dissipative transport properties of $(3+1)$ -dimensional Weyl semi-metals and Lorentz violating spinor electrodynamics. *ArXiv e-prints*, October 2012.
- [14] Gábor B. Halász and Leon Balents. Time-reversal invariant realization of the weyl semimetal phase. *Phys. Rev. B*, 85:035103, Jan 2012. doi: 10.1103/PhysRevB.85.035103.
- [15] T.T. Heikkila, N.B. Kopnin, and G.E. Volovik. Flat bands in topological media. *JETP Letters*, 94(3):233–239, 2011. ISSN 0021-3640. doi: 10.1134/S0021364011150045. URL <http://dx.doi.org/10.1134/S0021364011150045>.
- [16] P. Hosur, S. Ryu, and A. Vishwanath. Chiral topological insulators, superconductors, and other competing orders in three dimensions. *Phys. Rev. B*, 81(4):045120, 2010. doi: 10.1103/PhysRevB.81.045120.

- [17] Pavan Hosur. Friedel oscillations due to fermi arcs in weyl semimetals. *Phys. Rev. B*, 86:195102, Nov 2012. doi: 10.1103/PhysRevB.86.195102. URL <http://link.aps.org/doi/10.1103/PhysRevB.86.195102>.
- [18] Pavan Hosur, S. A. Parameswaran, and Ashvin Vishwanath. Charge transport in weyl semimetals. *Phys. Rev. Lett.*, 108:046602, Jan 2012. doi: 10.1103/PhysRevLett.108.046602.
- [19] D. Hsieh, D. Qian, L. A. Wray, Y. Xia, Y. S. Hor, R. J. Cava, and M. Z. Hasan. A topological Dirac insulator in a quantum spin Hall phase. 452:970–974, 2008. doi: 10.1038/nature06843.
- [20] H.-J. Kim, K.-S. Kim, J. F. Wang, M. Sasaki, N. Satoh, A. Ohnishi, M. Kitaura, M. Yang, and L. Li. Dirac vs. Weyl in topological insulators: Adler-Bell-Jackiw anomaly in transport phenomena. *ArXiv e-prints*, jul 2013.
- [21] C.-X. Liu, P. Ye, and X.-L. Qi. Chiral gauge field and axial anomaly in a Weyl semi-metal. *ArXiv e-prints*, April 2012.
- [22] L. Lu, L. Fu, J. D. Joannopoulos, and M. Soljačić. Weyl points and line nodes in gapless gyroid photonic crystals. *ArXiv e-prints*, July 2012.
- [23] Nobuki Maeda. Chiral anomaly and effective field theory for the quantum hall liquid with edges. *Physics Letters B*, 376:142 – 147, 1996. ISSN 0370-2693. doi: [http://dx.doi.org/10.1016/0370-2693\(96\)00274-2](http://dx.doi.org/10.1016/0370-2693(96)00274-2). URL <http://www.sciencedirect.com/science/article/pii/0370269396002742>.
- [24] Tobias Meng and Leon Balents. Weyl superconductors. *Phys. Rev. B*, 86:054504, Aug 2012. doi: 10.1103/PhysRevB.86.054504. URL <http://link.aps.org/doi/10.1103/PhysRevB.86.054504>.
- [25] Shuichi Murakami. Phase transition between the quantum spin hall and insulator phases in 3d: emergence of a topological gapless phase. *New Journal of Physics*, 9(9):356, 2007. URL <http://stacks.iop.org/1367-2630/9/i=9/a=356>.
- [26] H. B. Nielsen and M. Ninomiya. Absence of neutrinos on a lattice: (II). Intuitive topological proof. *Nuclear Physics B*, 193(1):173–194, 12 1981.
- [27] H. B. Nielsen and M. Ninomiya. The Adler-Bell-Jackiw anomaly and Weyl fermions in a crystal. *Physics Letters B*, 130(6):389 – 396, 1983. ISSN 0370-2693. doi: 10.1016/0370-2693(83)91529-0.
- [28] H.B. Nielsen and M. Ninomiya. Absence of neutrinos on a lattice: (i). proof by homotopy theory. *Nuclear Physics B*, 185(1):20 – 40, 1981. ISSN 0550-3213. doi: 10.1016/0550-3213(81)90361-8.
- [29] S. A. Parameswaran, T. Grover, D. A. Abanin, D. A. Pesin, and A. Vishwanath. Probing the chiral anomaly with nonlocal transport in Weyl semimetals. *ArXiv e-prints*, June 2013.
- [30] B. Rosenstein and M. Lewkowicz. Dynamics of electric transport in interacting weyl semimetals. *Phys. Rev. B*, 88:045108, Jul 2013. doi: 10.1103/PhysRevB.88.045108. URL <http://link.aps.org/doi/10.1103/PhysRevB.88.045108>.
- [31] D. T. Son and B. Z. Spivak. Chiral Anomaly and Classical Negative Magnetoresistance of Weyl Metals. *ArXiv e-prints*, June 2012.
- [32] F. F. Tafti, J. J. Ishikawa, A. McCollam, S. Nakatsuji, and S. R. Julian. Pressure Tuned Insulator to Metal Transition in $\text{Eu}_2\text{Ir}_2\text{O}_7$. *ArXiv e-prints*, July 2011.

- [33] A. M. Turner and A. Vishwanath. Beyond Band Insulators: Topology of Semi-metals and Interacting Phases. *ArXiv e-prints*, January 2013.
- [34] K. Ueda, J. Fujioka, Y. Takahashi, T. Suzuki, S. Ishiwata, Y. Taguchi, and Y. Tokura. Variation of charge dynamics in the course of metal-insulator transition for pyrochlore-type $\text{Nd}_2\text{Ir}_2\text{O}_7$. *Phys. Rev. Lett.*, 109:136402, Sep 2012. doi: 10.1103/PhysRevLett.109.136402. URL <http://link.aps.org/doi/10.1103/PhysRevLett.109.136402>.
- [35] O. Vafek and A. Vishwanath. Dirac Fermions in Solids - from High Tc cuprates and Graphene to Topological Insulators and Weyl Semimetals. *ArXiv e-prints*, June 2013.
- [36] M. M. Vazifeh and M. Franz. Electromagnetic response of weyl semimetals. *Phys. Rev. Lett.*, 111:027201, Jul 2013. doi: 10.1103/PhysRevLett.111.027201. URL <http://link.aps.org/doi/10.1103/PhysRevLett.111.027201>.
- [37] G.E. Volovik. *The Universe in a Helium Droplet*. International Series of Monographs on Physics. Oxford University Press, 2009. ISBN 9780199564842.
- [38] X. Wan, A. M. Turner, A. Vishwanath, and S. Y. Savrasov. Topological semimetal and fermi-arc surface states in the electronic structure of pyrochlore iridates. *Phys. Rev. B*, 83:205101, May 2011. doi: 10.1103/PhysRevB.83.205101.
- [39] Z. Wang and S.-C. Zhang. Charge Density Waves and Axion Strings from Weyl Semimetals. *ArXiv e-prints*, July 2012.
- [40] Z. Wang, H. Weng, Q. Wu, X. Dai, and Z. Fang. Three Dimensional Dirac Semimetal and Quantum Spin Hall Effect in Cd_3As_2 . *ArXiv e-prints*, May 2013.
- [41] Zhijun Wang, Yan Sun, Xing-Qiu Chen, Cesare Franchini, Gang Xu, Hongming Weng, Xi Dai, and Zhong Fang. Dirac semimetal and topological phase transitions in $A_3\text{Bi}$ ($a = \text{Na, k, rb}$). *Phys. Rev. B*, 85:195320, May 2012. doi: 10.1103/PhysRevB.85.195320. URL <http://link.aps.org/doi/10.1103/PhysRevB.85.195320>.
- [42] W. Witczak-Krempa and Y.-B. Kim. Topological and magnetic phases of interacting electrons in the pyrochlore iridates. *Phys. Rev. B*, 85:045124, Jan 2012. doi: 10.1103/PhysRevB.85.045124.
- [43] G. Xu, H. M. Weng, Z. Wang, X. Dai, and Z. Fang. Chern Semimetal and the Quantized Anomalous Hall Effect in HgCr_2Se_4 . *Phys. Rev. Lett.*, 107:186806, Oct 2011. doi: 10.1103/PhysRevLett.107.186806.
- [44] D. Yanagishima and Y. Maeno. Metal-nonmetal changeover in pyrochlore iridates. *Journal of the Physical Society of Japan*, 70(10):2880–2883, 2001. doi: 10.1143/JPSJ.70.2880.
- [45] K.-Y. Yang, Y.-M. Lu, and Y. Ran. Quantum hall effects in a weyl semimetal: Possible application in pyrochlore iridates. *Phys. Rev. B*, 84:075129, Aug 2011. doi: 10.1103/PhysRevB.84.075129.
- [46] S. M. Young, S. Zaheer, J. C. Y. Teo, C. L. Kane, E. J. Mele, and A. M. Rappe. Dirac semimetal in three dimensions. *Phys. Rev. Lett.*, 108:140405, Apr 2012. doi: 10.1103/PhysRevLett.108.140405. URL <http://link.aps.org/doi/10.1103/PhysRevLett.108.140405>.
- [47] Shou-Cheng Zhang and Jiangping Hu. A four-dimensional generalization of the quantum hall effect. *Science*, 294(5543):823–828, 2001. doi: 10.1126/science.294.5543.823. URL <http://www.sciencemag.org/content/294/5543/823.abstract>.

- [48] Jian-Hui Zhou, Jiang Hua, Niu Qian, and Shi Jun-Ren. Topological invariants of metals and the related physical effects. *Chinese Physics Letters*, 30(2):027101, 2013. URL <http://stacks.iop.org/0256-307X/30/i=2/a=027101>.
- [49] A. A. Zyuzin and A. A. Burkov. Topological response in Weyl semimetals and the chiral anomaly. *ArXiv e-prints*, June 2012.

This figure "MagnetoResistanceExpt.jpg" is available in "jpg" format from:

<http://arxiv.org/ps/1309.4464v1>

This figure "ParameswaranNonLocalTransport.jpg" is available in "jpg" format from

<http://arxiv.org/ps/1309.4464v1>